Atmospheric Entropy. Part I: Climate Dissipation Structure

JIANGNAN LI

Canadian Centre for Climate Modelling and Analysis, Science and Technology Branch, Environment Canada, University of Victoria, Victoria, British Columbia, Canada

PETR CHYLEK

Space and Remote Sensing Sciences, Los Alamos National Laboratory, Los Alamos, New Mexico

(Manuscript received 1 December 2010, in final form 26 October 2011)

ABSTRACT

Atmospheric entropy and its association with climate dissipation are investigated. The balance equation for entropy is derived through the mean and transient thermal and moisture equations. The entropy production contains the internal and external parts. The external entropy production, due to small-scale diabatic heating, can be evaluated by the surface entropy flux. Using NCEP data from 1998 to 2007, it is found that the surface entropy flux is much larger in the tropics than in the extratropics. In the December–February (DJF) Northern Hemisphere, there are two strong positive centers of boundary layer supply of entropy: one is in the northwestern Pacific and the other is in the western Atlantic. The external entropy production, due to large-scale eddy flow, can be evaluated by the convergence of eddy entropy flow. It is found that the large-scale eddy entropy flow is divergent in the midlatitudes and convergent in the higher latitudes. The internal entropy production shows the dissipation to the orderly thermal structure. For the internal entropy production due to a large-scale eddy, it is shown that in the Northern Hemisphere during DJF there are three maxima, located in the western Pacific, western Atlantic, and northern polar regions. This illustrates the dissipation of the highly organized thermal structure in such regions. An interesting finding is that the large-scale eddy internal entropy production is negative in the lower stratosphere. It is found that the long-time-averaged global mean of the internal entropy production is 0.037 49 W m^{-2} K^{-1}. By including the entropy sink from radiation, the total entropy production is close to balance.

1. Introduction

The nonequilibrium thermodynamics corresponding to climatological atmospheric entropy production is a fundamental problem that needs to be extensively explored.

In the last several decades, entropy, related to nonequilibrium thermodynamics, has been applied to various problems in the atmospheric sciences, for example, the general circulation of the atmosphere (Peixoto and Oort 1992; Johnson 1997; Goody 2000; Takamitsu and Kleidon 2005; Fraedrich and Lunkeit 2008; Pascale and Gregory 2009; Lucarini et al. 2011), moist convection (Pauluis and Held 2002a,b), and synoptic-scale severe atmospheric systems (Liu and Liu 2004). Additionally, Nicolis and Nicolis (1980) and Pujol and Llebot 1999b have applied the second differential of the entropy to instability in low-dimensional climate models. A significant effort has also been to study the maximum entropy production principle using simple climate models (Paltridge 1975; O'Brien and Stephens 1995; Pujol and Llebot 1999a; Lorenz et al. 2001; Ou 2001; Ozawa et al. 2003; Goody 2007; Shimokawa and Ozawa 2007; Li 2009; Lucarini 2009; Lucarini et al. 2010; and others).

Different from the equilibrium thermodynamics, which describes physics under the steady state condition, the nonequilibrium thermodynamics takes account of the time evolution of entropy as

$$\frac{d\rho s}{dt} \sim \frac{Q}{T},$$

where s is the entropy per unit mass, ρ is density, Q is the thermal heating rate, and T is the temperature. Since $Q \sim -\nabla \cdot \mathbf{J}$, where $\mathbf{J}$ is the thermal flow, we have

Corresponding author address: Dr. Jiangnan Li, Canadian Centre for Climate Modelling and Analysis, University of Victoria, P.O. Box 3065 STN CSC, Victoria BC V8W 3V6, Canada.
E-mail: jiangnan.li@ec.gc.ca

DOI: 10.1175/2011JCLI4234.1

$$\frac{d\rho s}{dt} \sim -\nabla \cdot \left(\frac{\mathbf{J}}{T}\right) + \mathbf{J} \cdot \nabla\left(\frac{1}{T}\right).$$

The first and the second terms are called the external and internal entropy production, respectively. The external entropy production deals with the local convergence (divergence) of the entropy flow $\mathbf{J}/T$. By Gaussian theorem, the volume integral of $\nabla \cdot (\mathbf{J}/T)$ can be transformed into a surface integral representing the flow across the boundary. Therefore, the external entropy provides the boundary entropy supply to a system. The internal entropy production describes the physics of dissipation, as flow $\mathbf{J}$ moving downgradient of temperature is an irreversible process, which reduces the orderliness of the system and is accompanied by positive internal entropy production. According to Prigogine (1980), dissipation is the most fundamental process in nature.

In the atmosphere, the corresponding entropy balance equation is much more complicated than the simple case discussed above. However, the basic physics should be similar. The atmosphere is a thermodynamic system containing many different physical processes. Most of them are irreversible, such as rainfall, convection, and transport of large-scale eddy flow, etc. These irreversible processes are associated with positive internal entropy production. Therefore, the orderliness of the atmosphere will decrease if the boundary does not provide enough negative entropy or if there is not a sufficient sink of entropy (due to radiation) inside the system. The main purpose of this work is to understand the boundary entropy supply and the convergence of entropy flow and to understand the extent of atmospheric internal entropy production and its impact on the climate's orderly appearance. To achieve this, the basic atmospheric entropy equation will be derived through the mean and transient thermal and moisture equations, in that all of the physical processes are included from the large scale to the small scale. Then, the basic entropy equation will be applied to the National Centers for Environmental Prediction–National Center for Atmospheric Research (NCEP–NCAR) reanalysis data (Kistler et al. 2001) to evaluate the atmospheric external and internal entropy production.

2. Theoretical background for atmospheric entropy

In an atmosphere containing dry air, water vapor, and liquid water (ice), the general governing equation for entropy (Iribarne and Godson 1981) is

$$ds = (1 - q_v - q_w)(c_{\mathrm{pd}} d \ln\theta) + (q_v c_{\mathrm{pv}} + q_w c_w) d \ln T + \frac{\lambda}{T} dq_v - q_v R_v d \ln\mathcal{H}, \quad (1)$$

where θ is the potential temperature; T is the temperature; q_v is the specific humidity for water vapor; q_w is the water mass mixing ratio; c_{pd} and c_{pv} are the specific heat at constant pressure for dry air and water vapor, respectively; c_w is the specific heat for water; R_v is the gas constant of water vapor; λ is the latent heat of evaporation of water; and $\mathcal{H}$ is the relative humidity. In the atmosphere, the typical values of q_v are less than 10^{-2} and $q_w < q_v$. Therefore, we can neglect $q_v + q_w$ in the first term and the whole second term in the right-hand side of (1). Hence, we have (Emanuel 1994) the following:

$$ds = c_{\mathrm{pd}} d \ln\theta + \frac{\lambda}{T} dq_v - q_v R_v d \ln\mathcal{H}. \quad (2)$$

From (2) we obtain the following entropy balance equation (details in the appendix):

$$\frac{\overline{d}(\rho\overline{s})}{dt} = -\frac{\partial}{\partial x_i}\left(\frac{J_{\theta i}}{\overline{\theta}} + \frac{J_{vi}}{\overline{T}} - R_v \frac{J_{vi}}{\lambda} \ln\overline{\mathcal{H}}\right) + -\frac{\partial}{\partial z}\left(\frac{\overline{F}_h}{\overline{T}} + \frac{\overline{F}_l}{\overline{T}} + \frac{\overline{F}_c}{\overline{T}} - \frac{\rho\overline{u}_\alpha \overline{\tau}_{3,\alpha}}{\overline{T}} - R_v \frac{\overline{F}_l + \overline{F}_m}{\lambda} \ln\overline{\mathcal{H}}\right) + \sigma + c_{\mathrm{pd}}\rho\frac{\overline{Q}_r}{\overline{T}}, \quad (3)$$

where the overbar and prime are the time mean and transient, respectively; $\overline{d}/dt = \partial/\partial t + \overline{u}_i \partial/\partial x_i$ is the Lagrangian derivative; $J_{\theta i}$ and J_{vi} are the large-scale eddy thermal flow and moistening heat flow, respectively; $\overline{F}_h$, $\overline{F}_l$, $\overline{F}_c$, and $\overline{F}_m$ are the mean sensible heat flux, latent heat flux, convective heat flux, and moistening heat flux, respectively; $\overline{\tau}_{i,j}$ is the mean diffusion acceleration tensor; and $\overline{Q}_r$ is the net radiative heating rate. In the right-hand side of (3), the first two terms are the external entropy productions due to the resolved large-scale eddy flow and the unresolved small-scale (subgrid scale) diabatic heat flux, respectively. The quantity σ is the internal entropy production shown in the appendix. The term $c_{\mathrm{pd}}\rho\overline{Q}_r/\overline{T}$ is a radiative entropy sink; since the global mean $\overline{Q}_r < 0$ in the atmosphere because the solar heating is generally less than infrared cooling. Without this negative radiation entropy production, the positive entropy production would accumulate to the maximum and the atmosphere would approach a random state without any climate phenomena.

In this paper, the subscript i (or j) takes values 1, 2, and 3, representing two horizontal and one vertical directions. For example, $x_1, x_2, x_3 = x, y, z$ for coordinates and $u_1, u_2, u_3 = u, v, w$ for velocities in the x, y, and z directions, etc. The subscript α takes the values 1 and 2, representing two horizontal directions. The convention of summing the repeated index i (or j) from 1 to 3 and the

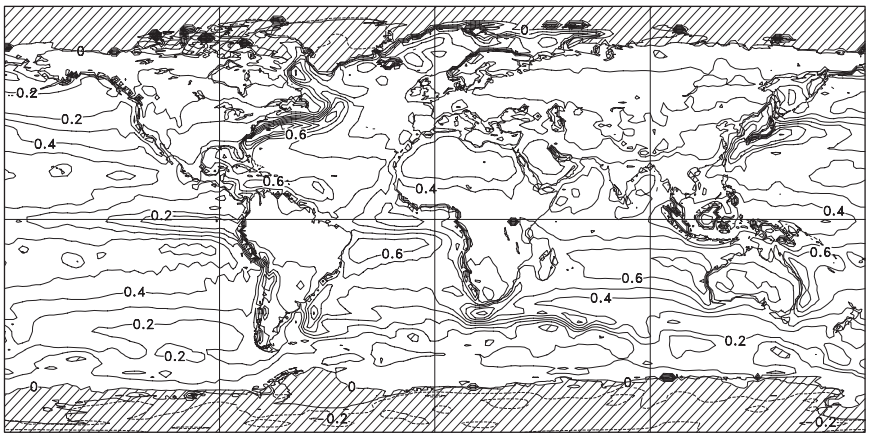

FIG. 1. Ten-year-averaged global distribution of the net surface entropy flux. Contour interval is 0.1 W m^{-2} K^{-1}, with negative contours shaded.

repeated index α from 1 to 2 is adopted, for example, $a_i b_i = a_1 b_1 + a_2 b_2 + a_3 b_3$ and $a_\alpha b_\alpha = a_1 b_1 + a_2 b_2$.

3. External entropy production—Surface entropy supply and convergence of eddy entropy flow

By applying vertical integration to (3), we obtain

$$\int_0^{z_t} \frac{\overline{d}(\rho\overline{s})}{dt} dz = \text{c.c.} + \left(\frac{\overline{F}_h}{\overline{T}} + \frac{\overline{F}_l}{\overline{T}} + \frac{\overline{F}_c}{\overline{T}} - \frac{\rho \overline{u}_\alpha \overline{\tau}_{3,\alpha}}{\overline{T}} - R_v \frac{\overline{F}_l + \overline{F}_m}{\lambda} \ln \overline{\mathcal{H}} \right)\Bigg|_{z=0} + \int_0^{z_t} \sigma \, dz + \int_0^{z_t} c_{\text{pd}} \rho \frac{\overline{Q}_r}{\overline{T}} dz, \tag{4}$$

where $z = 0$ is the surface, $z = z_t$ is the top of atmosphere (TOA), and c.c. implies the convergence contribution from large-scale eddies, which is defined as

$$\text{c.c.} = -\int_0^{z_t} \frac{\partial}{\partial x_i} \left(\frac{J_{\theta i}}{\overline{\theta}} + \frac{J_{vi}}{\overline{T}} - R_v \frac{J_{vi}}{\lambda} \ln \overline{\mathcal{H}} \right) dz. \tag{5}$$

It will show later that c.c. ≈ 0 for the global mean. Over a long time average, the global mean of the Lagrangian derivative of entropy should be close to zero as well. Therefore, in the sense of global mean,

$$\left\langle \left(\frac{\overline{F}_h}{\overline{T}} + \frac{\overline{F}_l}{\overline{T}} + \frac{\overline{F}_c}{\overline{T}} - \frac{\rho \overline{u}_\alpha \overline{\tau}_{3,\alpha}}{\overline{T}} - R_v \frac{\overline{F}_l + \overline{F}_m}{\lambda} \ln \overline{\mathcal{H}} \right)\Bigg|_{z=0} + \int_0^{z_t} \sigma \, dz + \int_0^{z_t} c_{\text{pd}} \rho \frac{\overline{Q}_r}{\overline{T}} dz \right\rangle_g \approx 0, \tag{6}$$

where $\langle \cdot \rangle_g$ represents a global mean. Locally, (6) does not hold.

Ten-year NCEP–NCAR monthly mean data from January 1998 to December 2007 are used to evaluate the boundary entropy supply and the atmospheric internal entropy production. The monthly data were interpolated into a 192 × 94 Gaussian grid, with 18 vertical levels that monotonically decrease with pressure from the surface up to 10 hPa. In the NCEP–NCAR reanalysis data, the three-dimensional large-scale eddy flows and the surface diabatic heat fluxes are provided. The unresolved small-scale diabatic heat fluxes within the atmosphere are not available but can be obtained from the diabatic heating rates by

$$F = c_{\text{pd}} \int_z^\infty \rho Q \, dz - F_{\text{TOA}} = \frac{c_{\text{pd}}}{g} \int_0^p Q \, dp - F_{\text{TOA}},$$

where g is the gravitation constant, F is the net diabatic heat flux at height z (or pressure p), Q is the corresponding diabatic heating rate, and F_{TOA} is the net flux at the top of the atmosphere. Here, F_{TOA} is zero for sensible, latent, and convective fluxes.

Figure 1 shows the global distribution of the 10-yr mean boundary supply of entropy by (6),

$$\left(\frac{\overline{F}_h}{\overline{T}} + \frac{\overline{F}_l}{\overline{T}} - \frac{\rho \overline{u}_\alpha \overline{\tau}_{3,\alpha}}{\overline{T}} - R_v \frac{\overline{F}_l}{\lambda} \ln \overline{\mathcal{H}} \right)\Bigg|_{z=0},$$

since the convective flux $\overline{F}_c|_{z=0} \approx 0$ for global mean is due to the cancellation of updrafts and downdrafts near the surface. In the atmosphere, heat release by convective condensation occurs mostly in the midtroposphere, resulting in a relatively large convective flux there.

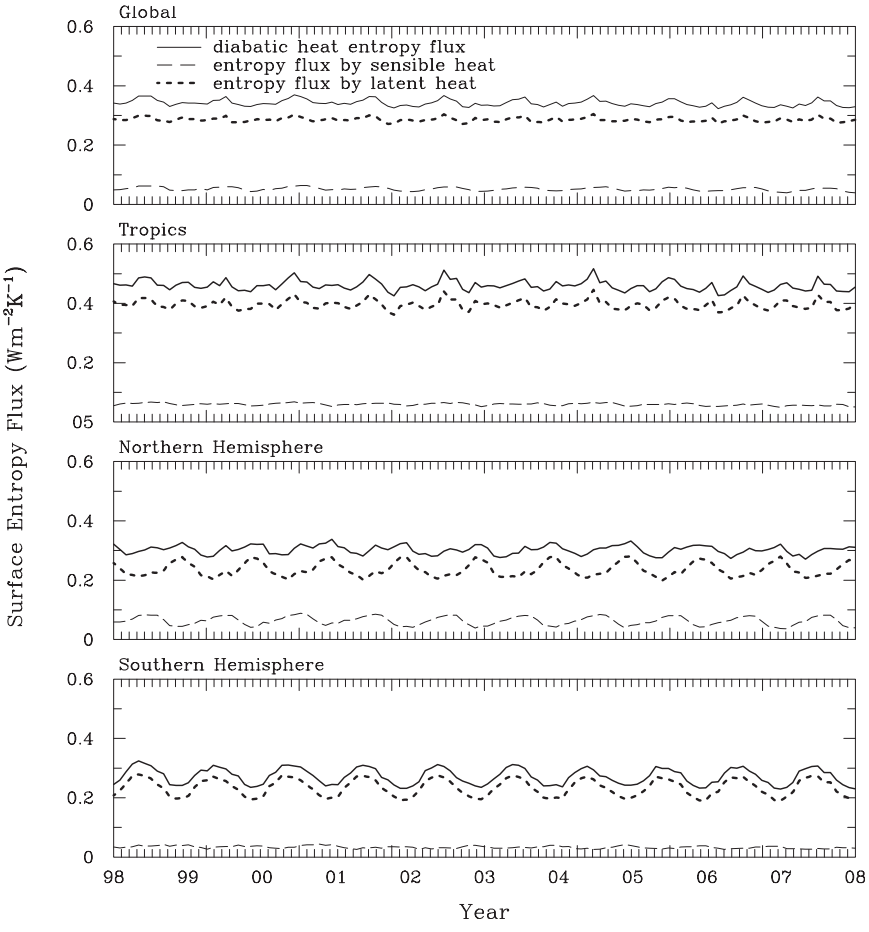

FIG. 2. Solid lines show the 10-yr time evolution of the net entropy flux for global and regional means. Dashed lines and dotted lines are the same as the solid lines but for surface entropy flux due to sensible heat and latent heat, respectively.

It is seen in Fig. 1 that in the tropics and lower-latitude regions, the boundary supply of entropy is generally positive; only in the northern and southern polar regions is the boundary supply of entropy in weakly negative value. The distribution of the entropy supply is very nonhomogeneous. Over large areas of the Atlantic Ocean and the Indian Ocean, the surface entropy supply is in the range of 0.4–0.6 W m^{-2} K^{-1}. Over the tropical ocean near South America, there is an elongated region with a relatively low entropy supply, with a value as low as 0.1 W m^{-2} K^{-1}. In such regions there is strong upwelling of cold water from the deep ocean, which leads the weak upwelling sensible/latent heat flux and surface entropy supply.

There are two regions with very high boundary entropy supply: one is in the northwestern Pacific and the other is in the northwestern Atlantic near the eastern coast of North America. In these two regions, the surface entropy fluxes are greater than 0.8 W m^{-2} K^{-1}. These are regions where warm ocean western boundary currents (the Kuroshio and the Gulf Stream) tend to warm the atmosphere.

Figure 2 shows the time evolution of the global mean boundary supply of entropy. Additionally, the regional mean results are shown for the tropics (18°S–18°N), the Northern Hemisphere (18°–90°N), and the Southern Hemisphere (18°–90°S). It is found that the global mean boundary entropy flux is close to 0.35 W m^{-2} K^{-1} with a weakly seasonal oscillation. The time-averaged value is listed in Table 1. Since the boundary supply of entropy is dominated by the latent heat and sensible heat, the results of boundary entropy fluxes by the latent heat and sensible heat are also shown in Fig. 2.

In the tropics the boundary supply entropy flux is large, but the seasonal oscillation is weak. Outside of the tropics, in both the Northern and Southern Hemispheres, the boundary supplies of the entropy flux are smaller than those of the tropics; however, the seasonal

TABLE 1. Global mean and regional mean of the net boundary entropy supply for individual physical processes (W m^{-2} K^{-1}).

		Global	Tropics (18°S–18°N)	Northern Hemisphere (18°–90°N)	Southern Hemisphere (18°–90°S)
Sensible heat	$\left.\frac{\overline{F}_h}{\overline{T}}\right\|_{z=0}$	0.0521	0.0597	0.0631	0.0335
Latent heat	$\left.\frac{\overline{F}_l}{\overline{T}}\right\|_{z=0}$	0.2860	0.3961	0.2366	0.2340
Surface evaporation	$\left.-R_v\frac{\overline{F}_l}{\lambda}\ln\overline{\mathcal{H}}\right\|_{z=0}$	0.0026	0.0035	0.0022	0.0021
Stress	$\left.-\frac{\rho\overline{u}_\alpha\overline{\tau}_{3,\alpha}}{\overline{T}}\right\|_{z=0}$	0.0015	0.0011	0.0010	0.0025
Total	$\|_{z=0}$	0.3422	0.4604	0.3029	0.2721

oscillations become larger, especially in the Southern Hemisphere. By decomposing the entropy flux into the latent heat and sensible heat components, strong seasonal oscillations are found for both parts in the Northern and Southern Hemispheres, but their phases are different. In the winter season of the Northern Hemisphere, the surface latent heat flux is relatively high and the surface temperature is relatively low. Both factors contribute a higher surface entropy flux. However, the relatively low surface temperature can cause the low surface sensible flux and its related entropy flux. Therefore, the phases of the surface entropy flux are different for the latent heat and sensible heat parts. This difference in phase results in a weak seasonal oscillation in the total. The same is true for the summer season. In the Southern Hemisphere, the seasonal oscillation of the surface entropy flux is strong, since the total result is mainly determined by the latent heat part.

Table 1 lists the 10-yr mean values of entropy supply corresponding to latent heat, sensible heat, irreversible surface evaporation, and surface stress. The term $-R_v(\overline{F}_l/\lambda)\ln\overline{\mathcal{H}}|_{z=0}$ is the irreversible surface evaporation and corresponds to the production of entropy flux by surface evaporation under the nonsaturation condition of $\overline{\mathcal{H}} < 1$, which is an irreversible process. Though this term is small, it is larger than the surface stress term.

To comprehend the seasonal pattern, Fig. 3 shows the net surface entropy flux for the December–February (DJF) Northern Hemisphere (or called boreal winter) and the June–August (JJA) Southern Hemisphere (or called austral winter). The corresponding zonal mean values are plotted in the bottom panels. Compared to the JJA Southern Hemisphere, the DJF Northern Hemisphere shows more structure. In the DJF Northern Hemisphere, there are two strong positive centers: one is in the northwestern Pacific and the other is in the western Atlantic near the coast of North America corresponding to the Kuroshio and the Gulf Stream. In the two contour centers, the entropy fluxes are greater than 1.6 W m^{-2} K^{-1}, while in the other regions the surface entropy supply is more homogeneous and relatively small. In the JJA Southern Hemisphere, the main structure of the net surface entropy flux is a large circle of entropy flux over 0.2 W m^{-2} K^{-1} around 30°–50°S. There is a negative surface entropy flux in the Antarctic polar region, which is due to the negative (downward) surface sensible heat flux over regions covered with sea ice and snow.

The second part of the external entropy production is due to large-scale eddies, the c.c term in (5). The global mean of c.c. is zero, since by Gaussian theorem we have

$$\langle \text{c.c.}\rangle_g \sim -\int\int dx\,dy\int_0^{z_t} dz\,\frac{\partial}{\partial x_i}\left(\frac{J_{\theta i}}{\overline{\theta}}+\frac{J_{vi}}{\overline{T}}-R_v\frac{J_{vi}}{\lambda}\ln\overline{\mathcal{H}}\right)$$
$$= -\oint_\Omega d\Sigma_i\left(\frac{J_{\theta i}}{\overline{\theta}}+\frac{J_{vi}}{\overline{T}}-R_v\frac{J_{vi}}{\lambda}\ln\overline{\mathcal{H}}\right)=0, \quad (7)$$

where $d\Sigma_i$ is the surface integral element in the i direction and Ω is the integral area covering the atmosphere, that is, the boundary of the surface and the boundary of the TOA. The integral of (7) is zero under the condition that $J_{\theta i} = J_{vi} = 0$ at the surface and the TOA. This condition is usually assumed in large-scale dynamics (James 1994).

Figure 4 shows the distribution of c.c. for the DJF Northern Hemisphere and the JJA Southern Hemisphere (top panels). The calculation is based on (5). Since the NCEP data are only up to 10 hPa, the upper limit of the integral is set to z_m, where z_m is the height at 10 hPa. Generally the values are negative in the lower-latitude regions and become positive in the higher-latitude regions. This indicates that the large-scale eddy entropy flow is divergent in the lower-latitude regions and convergent in the higher-latitude regions.

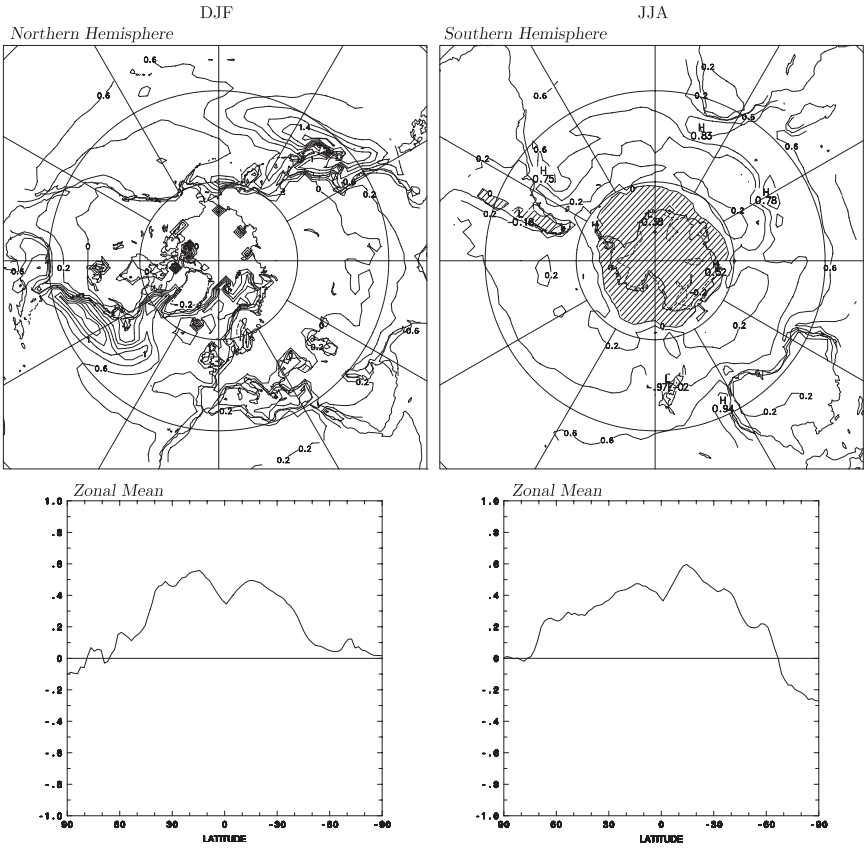

FIG. 3. (top) Distributions of the surface entropy flux for (left) the DJF Northern Hemisphere and (right) the JJA Southern Hemisphere. Contour interval is 0.2 W m $^{-2}$ K^{-1} with negative contours shaded. (bottom) Zonal mean surface entropy flux is shown for (left) DJF and (right) JJA (W m^{-2} K^{-1}).

In the top-left panel of Fig. 4, it is shown that the large divergences occur in the northwestern Pacific and western Atlantic near the coast of North America. They are close to the locations with large positive values of the surface entropy flux displayed in Fig. 3. It is the strong local surface entropy supply that causes the strong local divergence of the entropy flow in these regions, since the system tends to reach a balance in entropy production. It is interesting to note that the two strong convergent centers are near to the two strong divergent centers, as the poleward entropy flow gradually converges in the transport process. Similar to the surface entropy supply case, the JJA Southern Hemisphere shows less structure for the entropy convergence.

The corresponding zonal mean results are presented in the bottom panels of Fig. 4. It is clearly shown that the local maxima of the divergences of entropy occur at about 30° in the winter hemisphere and at about 40° in the summer hemisphere for both DJF and JJA. The divergence of the large-scale eddy entropy flow in the midlatitudes and the convergence of it in the higher latitudes works as the meridional transport of the entropy flow, since the polar regions have large entropy sink because of the longwave cooling as the term of $c_{\mathrm{pd}}\rho\overline{Q}_r/\overline{T}$ in (6).

4. Internal entropy production—Climate dissipation

The atmospheric internal entropy production given in the appendix is

$$\sigma = J_{\theta i}\frac{\partial}{\partial x_i}\frac{1}{\overline{\theta}} + J_{vi}\frac{\partial}{\partial x_i}\frac{1}{\overline{T}} - R_v\frac{J_{vi}}{\lambda}\frac{\partial \ln\overline{\mathcal{H}}}{\partial x_i} + (\overline{F}_h + \overline{F}_l + \overline{F}_c)\frac{\partial}{\partial z}\frac{1}{\overline{T}} - \overline{u}_\alpha\frac{\partial}{\partial z}\left(\frac{\rho\overline{\tau}_{3,\alpha}}{\overline{T}}\right) - R_v\frac{\overline{F}_l + \overline{F}_m}{\lambda}\frac{\partial \ln\overline{\mathcal{H}}}{\partial z} + R_v\rho(\overline{C - E})\ln\overline{\mathcal{H}}. \quad (8)$$

The first two terms of (8) refer to the large-scale eddy thermal flow and the moistening heat flow, the third term is due to the diffusion of the large-scale eddy

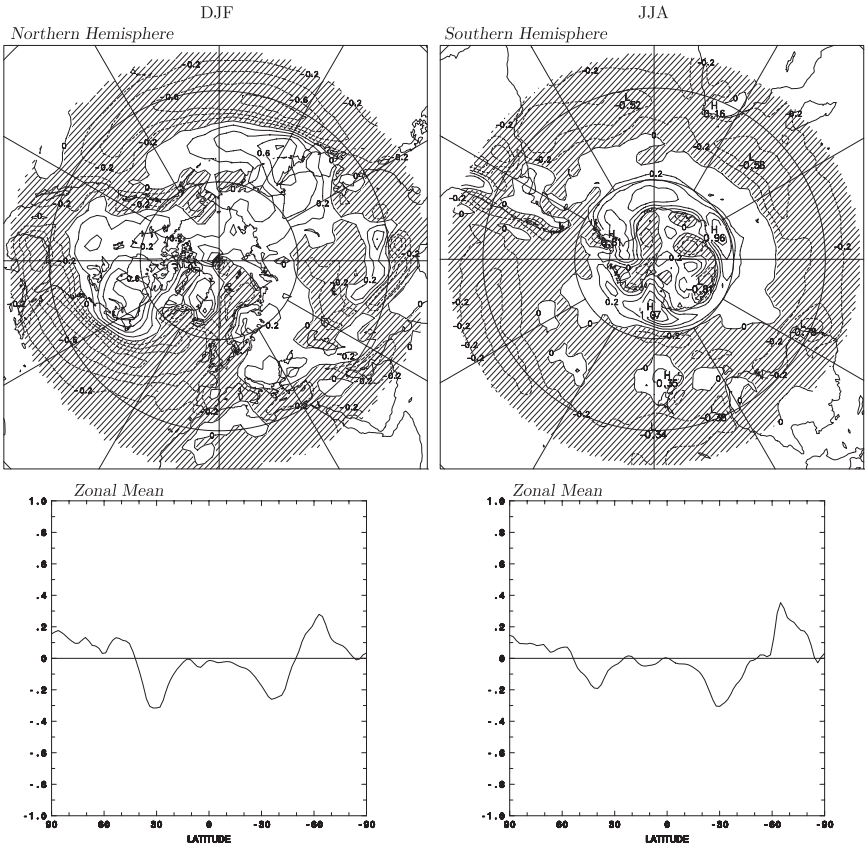

FIG. 4. As in Fig. 3, but for vertically integrated convergence of entropy.

moisture flow, the forth term is due to the small-scale diabatic heat fluxes, the fifth term is due to small-scale viscous stress, the sixth and last terms are due to the diffusion of the small-scale moisture flux and irreversible condensation–evaporation.

Internal entropy production illustrates the relationship between the gradient of mean fields (temperature, potential temperature, and moisture as shown in $\ln\overline{\mathcal{H}}$) and large-scale eddy flows and small-scale diabatic heat fluxes. There is probably no other physical quantity that can be associated with so many physical variables. Usually a compound physical quantity is suitable to describe a complicated physical process: potential vorticity (PV) being a good example. Therefore, entropy, especially the internal entropy production, is expected to be able to describe various climate–weather phenomena.

Let us consider a simple case of thermal flow only, from de Groot and Mazur (1984); the corresponding internal entropy production is

$$\sigma = J_i \frac{\partial}{\partial x_i}\frac{1}{T}, \tag{9}$$

and by Fourier's law the thermal flow is

$$J_i = -k\frac{\partial T}{\partial x_i}, \tag{10}$$

where k is the diffusivity. Hence, we obtain $\sigma = k(1/T^2)(\partial T/\partial x_i)^2 > 0$. This shows that the internal entropy must be positive for an irreversible process, since in (10) the thermal flow moving along the downgradient of temperature is irreversible.

Equation (10) shows that the flow moves along the temperature gradient from the higher-temperature region to the lower-temperature region. During this process, the flow tends to smooth out the gradient of the temperature field by extracting energy from the high-temperature regions. This results in the redistribution of the temperature profile and the reduction of the existing slope of temperature. Therefore, the positive internal entropy production is referred to as dissipation (de Groot and Mazur 1984).

In the atmosphere, the structure in the temperature field is always present because of the nonhomogeneous distribution of radiative heating. A region with large internal entropy production corresponds to a large dissipative process. This indicates that in such a region, there

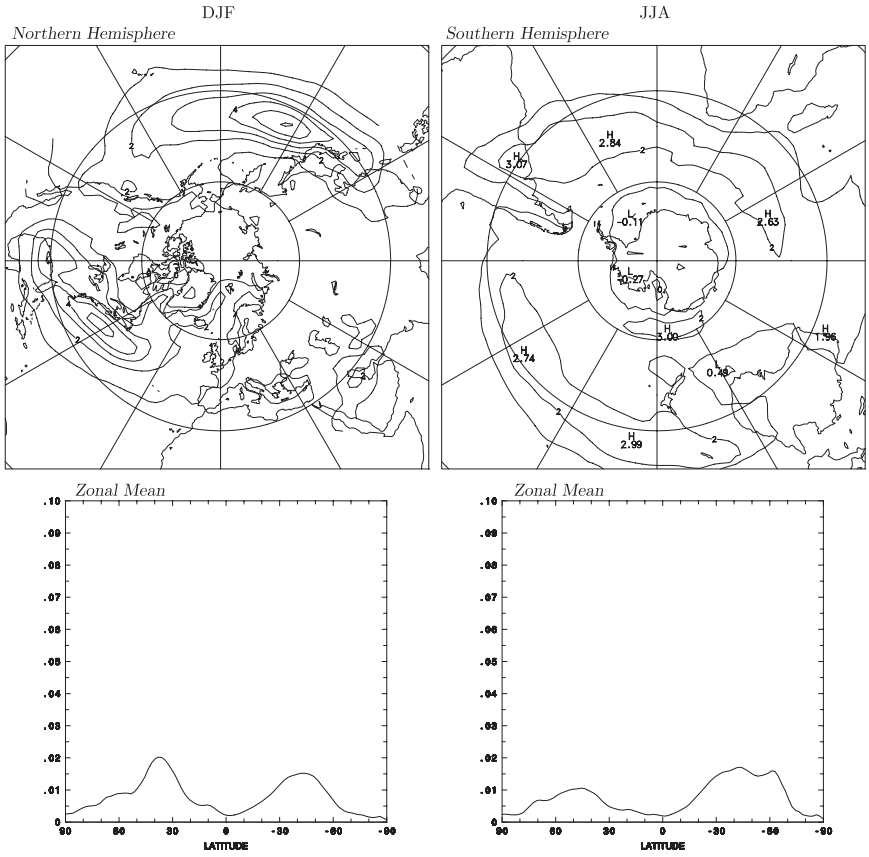

FIG. 5. As in Fig. 3, but for vertically integrated internal entropy production due to large-scale eddies. Calculations are based on (11).

is a highly organized temperature structure that can be dissipated. Otherwise, the dissipation process cannot last long. From this point of view, a region of positive internal entropy production must correlate with the dissipative temperature structure.

We first discuss the internal entropy production by large-scale eddy flows based on (8),

$$\sigma = J_{\theta i}\frac{\partial}{\partial x_i}\frac{1}{\overline{\theta}} + J_{vi}\frac{\partial}{\partial x_i}\frac{1}{T} - R_v\frac{J_{vi}}{\lambda}\frac{\partial \ln \overline{\mathcal{H}}}{\partial x_i}. \qquad (11)$$

The top panels of Fig. 5 show the distribution of vertically integrated internal entropy production by (11) for the DJF Northern Hemisphere and the JJA Southern Hemisphere.

In the DJF Northern Hemisphere, there are well-defined patterns of internal entropy production with two maximum centers in the northwestern Pacific and the northwestern Atlantic. Based on the above discussions, there must be orderly atmospheric thermal structures in such regions that are being continuously dissipated. In the JJA Southern Hemisphere, there are large internal entropy productions in the polar region as well as in the subtropical high pressure region. In the bottom panels of Fig. 5, the corresponding zonal mean results of the vertically integrated internal entropy production are shown. It is seen that the maximum regions are in the midlatitudes for both the Northern and Southern Hemispheres.

To understand the correlation between the large-scale eddy flow and the gradient of temperature in internal entropy production and to understand to what extent the relationship of the form of (10) holds in the atmosphere, we present the distribution of the vertical mean gradient of temperature as $\langle \partial \overline{T}/\partial y \rangle_p$ in Fig. 6. The vertical mean is defined as

$$\left\langle \frac{\partial \overline{T}}{\partial y} \right\rangle_p = \frac{1}{p_s}\int_0^{p_s} \frac{\partial \overline{T}}{\partial y}\, dp, \qquad (12)$$

where p_s is the surface pressure. Equation (12) is equivalent to a mass-weighted mean. In addition, the distributions of the vertical mean large-scale eddy thermal flow $\langle c_{\mathrm{pd}}\overline{T'v'}_p \rangle$ and the large-scale eddy moistening heat flow $\langle \lambda \overline{q'v'} \rangle_p$ are plotted. We discuss only the case of latitudinal contributions, since they are much larger than the longitudinal contributions.

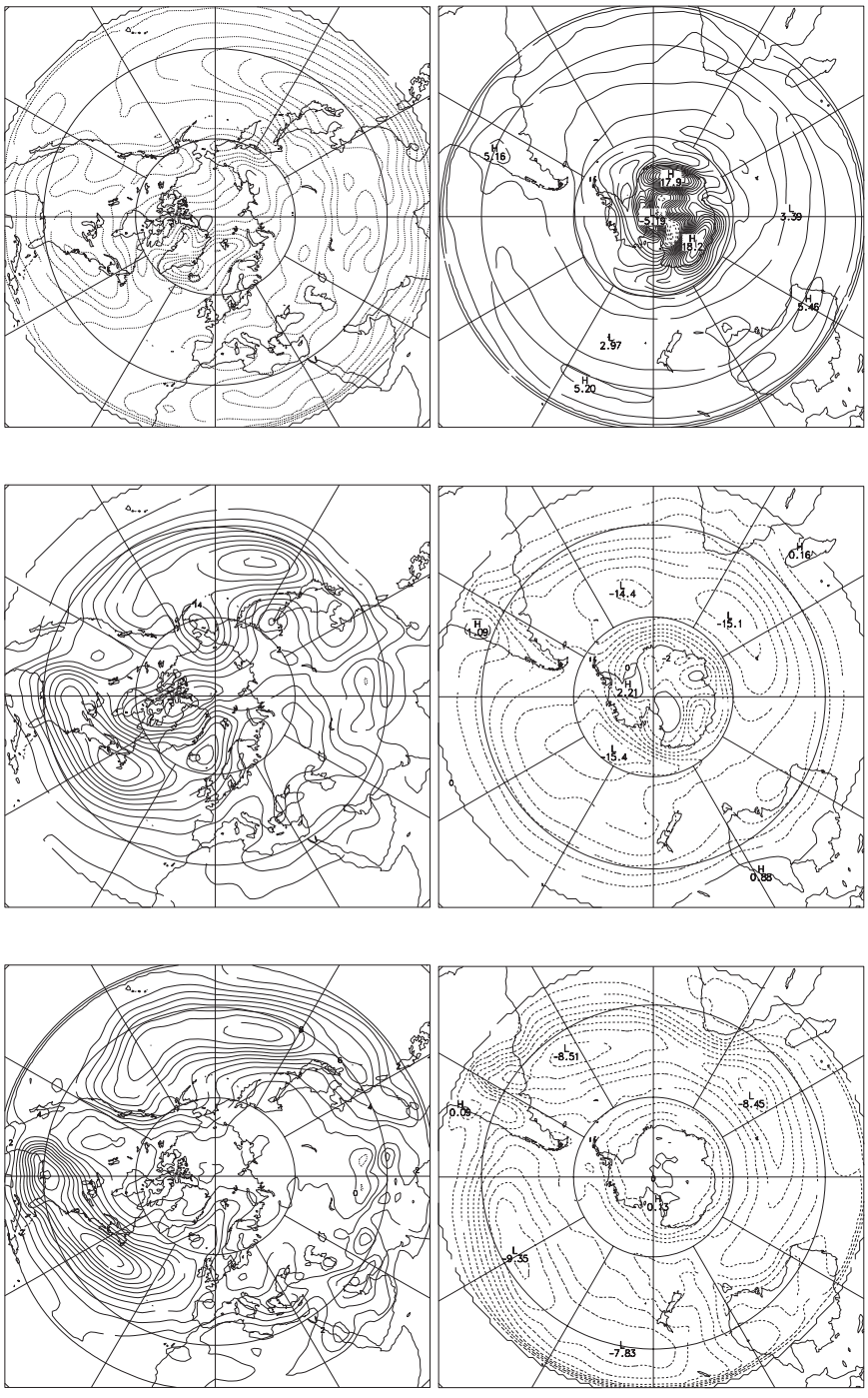

FIG. 6. Distributions of pressure-averaged gradient $\langle \partial \overline{T}/\partial y \rangle_p$ (K m^{-1}), eddy thermal flow $\langle c_{pd} \overline{T'v'} \rangle_p$ (K m^{-1}), and eddy moistening heat flow $\langle \lambda \overline{q'v'} \rangle_p$ (W m^{-2}).

The top panels of Fig. 6 show the distribution of the vertical mean latitudinal temperature gradient. In the DJF Northern Hemisphere, there are three centers located in the regions close to the centers of internal entropy production shown in Fig. 5. In addition, the pattern of the JJA Southern Hemisphere is similar to that of the internal entropy production. The bottom two rows of Fig. 6 show the distribution of the vertical mean eddy flows in the latitudinal direction. In the DJF Northern Hemisphere, there are strong correlations

between the temperature gradient and the eddy flows, especially in the western Atlantic region. Therefore, the linear proportion of the eddy flows of $\langle c_{\rm pd}\overline{T'v'_p}\rangle$ and $\langle\lambda\overline{q'v'}\rangle_p$ to the temperature gradient $\langle\partial\overline{T}/\partial y\rangle_p$ indicates that (10) indeed holds to some extent in the atmosphere. As discussed above, the correlated eddy flows try to smooth out the existing temperature structures. In the atmosphere, this kind of eddy flow does exist, especially in the latitudinal direction.

In fact, the relationship of (10) has been studied as the macroturbulence diffusion in Held (1999). Readers are referred to it for a detailed physical discussion. In Fig. 2 of Held (1999), a result at 850 hPa was shown for $c_{\rm pd}\overline{T'u'_i} \sim -\partial\overline{T}/\partial x_i$ that is similar to the result of Fig. 6. What we presented here is the mass-weighted vertical integrated result, which shows that this diffusion relation seems to be true for the whole troposphere. In addition, it is shown in Fig. 6 that the large-scale eddy moistening heat flow $\langle\lambda\overline{q'v'}\rangle_p$ also follows this type of macroturbulence diffusion.

Besides the thermal structure, internal entropy production is also associated with the dynamical structure. Since the temperature gradient is much larger in the latitudinal direction than in the longitudinal direction. It follows that for large-scale eddy flow,

$$\sigma \sim c_{\rm pd}\rho(\overline{\theta'v'})\frac{\partial}{\partial y}\frac{1}{\overline{\theta}} + \lambda\rho(\overline{q'v'})\frac{\partial}{\partial y}\frac{1}{\overline{T}}. \tag{13}$$

In the midlatitudes, the quasigeostrophic theory yields the thermal wind relation $\partial\theta/\partial y \sim \partial u/\partial p$. Then, the first term on the right-hand side of (13) is

$$\begin{aligned}\int_0^\infty \sigma\, dz &\sim -\int_0^{p_s}\frac{(\overline{\theta'v'})}{\overline{\theta}^2}\frac{\partial\overline{u}}{\partial p}dp\\ &= -\frac{(\overline{\theta'v'})\overline{u}}{\overline{\theta}^2}\bigg|_{p_s} + \frac{(\overline{\theta'v'})\overline{u}}{\overline{\theta}^2}\bigg|_0 + \int_0^{p_s}\frac{\partial}{\partial p}\left[\frac{(\overline{\theta'v'})}{\overline{\theta}^2}\right]\overline{u}\,dp\\ &= \int_0^{p_s}\frac{\partial}{\partial p}\left[\frac{(\overline{\theta'v'})}{\overline{\theta}^2}\right]\overline{u}\,dp,\end{aligned} \tag{14}$$

since $\overline{u} = 0$ at the boundaries of $p = p_s$ and 0. Generally, in the midlatitude region above the boundary layer, the poleward thermal flow, $\overline{\theta'v'}$, decreases with height and $\overline{\theta}$ increases with height; hence, $\partial/\partial p[(\overline{\theta'v'})/\overline{\theta}^2] > 0$. Therefore,

$$\int_0^\infty \sigma\, dz \sim \int_0^{p_s}\overline{u}\,dp \sim \langle\overline{u}\rangle_p. \tag{15}$$

A similar relationship holds for the second term on the right-hand side of (13). Therefore, in the midlatitude westerly regions, the large-scale eddy internal entropy production is likely to be positive. The result of (15) is supported by the distribution of $\overline{u}$ at 250 hPa in the DJF Northern Hemisphere and the JJA Southern Hemisphere [Fig. 6.15 in James (1994)]. Our calculations also show that for the winter Northern Hemisphere, $\langle\overline{u}\rangle_p$ has two large maxima, one located in the northwestern Pacific and the other in the western Atlantic near the coast of North America, nearly in the same locations as the two high internal entropy production areas shown in Fig. 5.

Therefore, (13) describes the typical dissipation process in which the eddy flow acts to redistribute the temperature and dynamical structures. This process tends to irreversibly change the system from order to disorder and thus corresponds to an increase of internal entropy production. As mentioned above, the temperature gradient is mostly created by the nonhomogeneous distribution of radiation energy. Therefore, it is the radiation that maintains the temperature and dynamical structures and the eddy flow tends to dissipate them. Regionally, the air–sea interactions at the western boundary currents also help maintain the atmospheric temperature structure due to strong ocean fronts there. As it is shown above, the strong dissipation structures occur in the northwestern Pacific near Japan and near the eastern coast of North America, which indicates the maintained orderly temperature structures in these western boundary regions.

The vertical distribution of the zonal mean internal entropy production due to large-scale eddy flows is shown in the top panels of Fig. 7 for DJF and JJA. In DJF, below 250 hPa there are two centers of large internal entropy production. These occur at about 40°N and 45°S, coincident with the regions of large-scale eddy kinetic energy (James 1994). Large-scale eddy meridional heat flows are found in these regions of large meridional temperature gradient, where the eddies act against the temperature gradient to make it smaller than it would otherwise be.

In JJA, there is also a large internal entropy production within the boundary layer around altitude 60°–75°S. The detailed analysis shows that the large internal entropy production is mostly produced by the dissipation in the meridional direction, as the term of $c_{\rm pd}\rho(\overline{\theta'v'})\partial(1/\overline{\theta})/\partial y$. In the austral winter, the sea ice extends close to 60°S. A large meridional temperature gradient of $\partial\overline{\theta}/\partial y$ is found over the sea ice–covered regions.

It is very interesting to find that there is negative internal entropy production in the lower stratosphere, though the value is very small. The negative internal entropy production in the lower stratosphere is mainly produced by the large-scale eddy thermal flow in the latitudinal direction as the large-scale eddy thermal flow

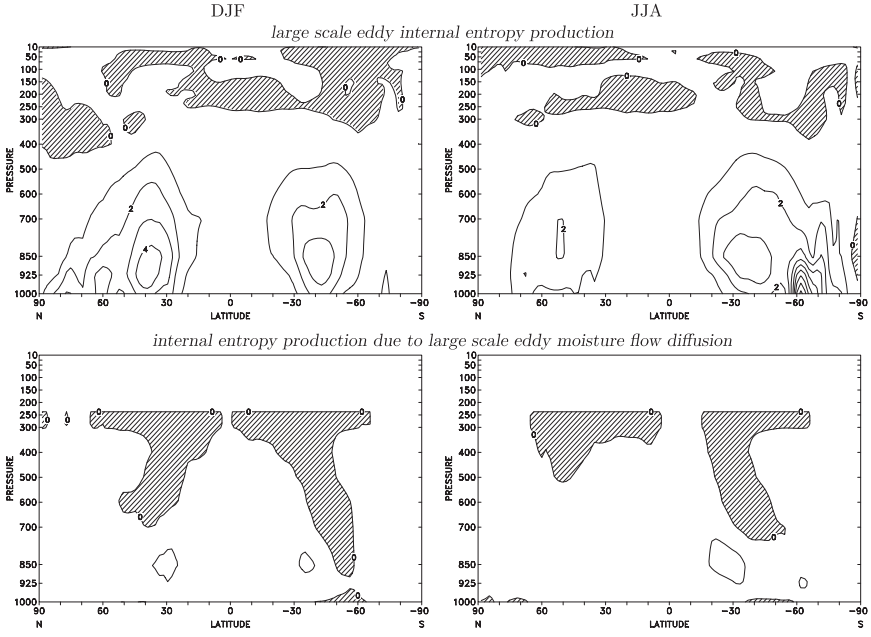

FIG. 7. (top) Vertical distributions of zonal mean internal entropy production due to large-scale eddy for (left) DJF and (right) JJA. (bottom) Vertical distributions of zonal mean internal entropy production due to diffusion of large-scale eddy moisture flow only. Contour interval is 10^{-6} W m^{-3} K^{-1} with negative contours shaded.

moves along the countergradient of temperature. The large-scale eddy flow comes from the temporal variation. Therefore, the large-scale eddy flows in the lower stratosphere are not directly driven by the temperature gradient as shown in (10), which is necessary for a positive internal entropy production as discussed above.

The countergradient large-scale eddy thermal flow has been discussed previously (Wallace 1978). Understanding this phenomenon from an atmospheric entropy point of view has not been addressed. The negative entropy production results indicate that large-scale eddies have very weak correlation to the temperature gradient in the lower stratosphere. Thus, the relation of (10) does not hold true as that shown in Fig. 6.

The eddy moisture flow diffusion term $-R_v(J_{vi}/\lambda)\,\partial \ln \overline{\mathcal{H}}/\partial x_i$ shows the internal entropy production is due to the eddy moisture flow J_{vi}/λ moving along the gradient of $\overline{\mathcal{H}}$. This is similar to $-J_i \partial T/\partial x_i$ in (9), which shows the internal entropy production is due to the thermal flow J_i moving along the gradient of T. The vertical distribution of the zonal mean internal entropy production due to eddy moisture flow diffusion is shown in the bottom panels of Fig. 7. The result is only up to 200 hPa, since the NCEP data of $\mathcal{H}$ are limited to 200 hPa. It is shown that the entropy production due to eddy moisture diffusion is very small in comparison to the other two large-scale eddy terms in (11). Also, it is found that the internal entropy production due to eddy moisture diffusion can be very weakly negative. In such cases, the eddy moisture flow is forced to move from a lower $\mathcal{H}$ region to a higher $\mathcal{H}$ region.

The dissipation corresponding to large-scale eddies is a very distinctive characteristic of atmospheric entropy. Generally for a physical variable ψ such as water vapor, temperature, etc., the balance equation for its mean is

$$\frac{\overline{d}\,\overline{\psi}}{dt} = -\frac{\partial(\overline{u_i'\psi'})}{\partial x_i} + \overline{O},$$

where O is the unresolved small-scale source. In the global mean,

$$\left\langle \int_0^{z_t} \frac{\partial \overline{\psi}}{\partial t}\, dz \right\rangle_g = \left\langle \int_0^{z_t} \overline{O}\, dz \right\rangle_g,$$

provided $\overline{u} = \overline{u_3'\psi'} = 0$ at the surface and the TOA. Therefore, in the global mean, large-scale eddies have no contribution to the production of $\overline{\psi}$, since the large-scale circulation does not increase the amount of ψ. This is very different from the entropy case. Even for the global mean, large-scale eddies contain the contribution to the entropy production as shown above. Entropy is a measure of the orderliness of a thermodynamic system. Any irreversible motion will lead to an increase of entropy, since the irreversible motion dissipates the orderliness of the system.

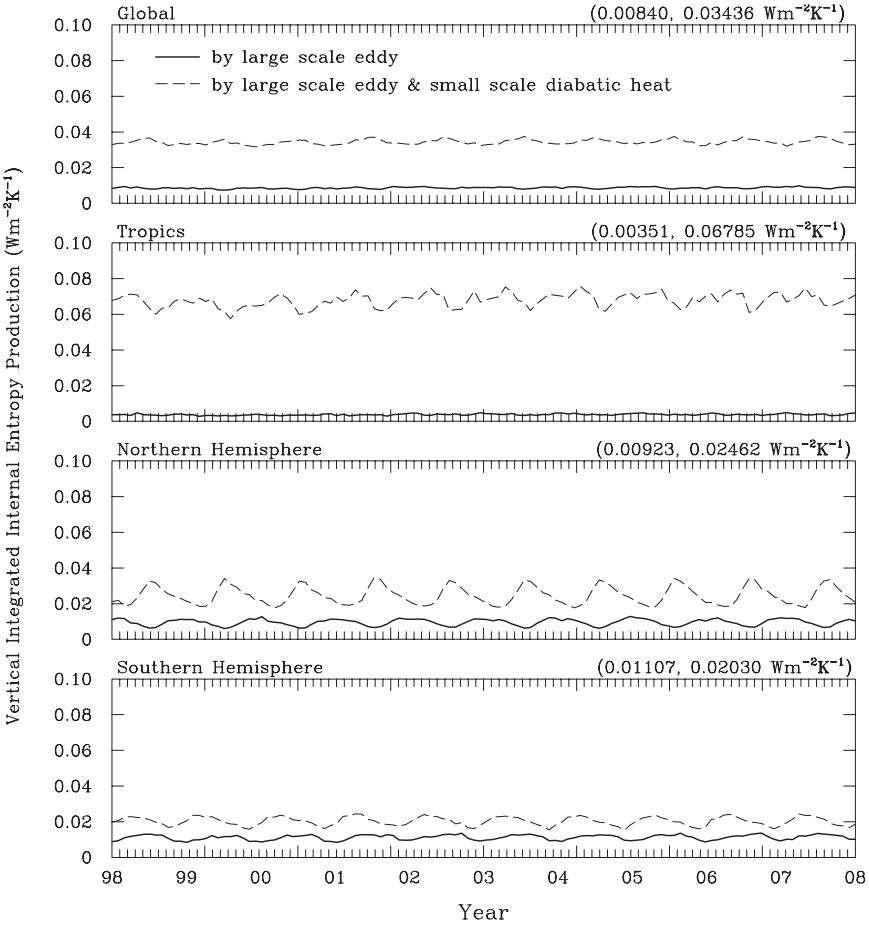

FIG. 8. Solid lines show 10-yr time evolution of the vertically integrated internal entropy production due to large-scale eddy for global and regional means. Dashed lines show corresponding results for internal entropy production due to large-scale eddy and small-scale diabatic heat. In the parentheses above each panel, the first and second numbers are the time-averaged values for large-scale eddy and for large-scale eddy plus small-scale diabatic heat, respectively.

The time evolution of the vertically integrated large-scale eddy internal entropy production is presented in Fig. 8, with the global mean and three regional means. In the tropics, the curve is very flat and its value is very small. For both the Northern and Southern Hemispheres, the result is always larger in the winter hemisphere, since large-scale eddies are generally stronger in the winter season. The time-averaged global mean and the regional mean values are also shown in Fig. 8.

Now we investigate the total internal entropy production corresponding to both large-scale eddy flows and small-scale diabatic heat fluxes based on (8). Takamitsu and Kleidon (2005) have addressed the effect of small-scale diabatic heat fluxes. In Fig. 9 the vertically integrated total internal entropy production is shown for the DJF Northern Hemisphere and the JJA Southern Hemisphere. Three maxima were found in the DJF Northern Hemisphere. These centers are found in the western Pacific, the western Atlantic, and the polar region (in the Atlantic sector), similar to the result for large-scale eddies only.

For the zonal mean result shown in the bottom panels of Fig. 9, the internal entropy production has large values in the tropical region, which is different from that of the internal entropy production by the large-scale eddy only, as shown in Fig. 5.

In the JJA Southern Hemisphere, the positive internal entropy production shows large centers around Antarctica. The pattern is similar to that of the boundary entropy supply shown in the top panels of Fig. 3. The corresponding zonal mean result in the bottom panel also shows a peak value in the tropical region.

The vertical distribution of the zonal mean total internal entropy production is shown in the top panels of

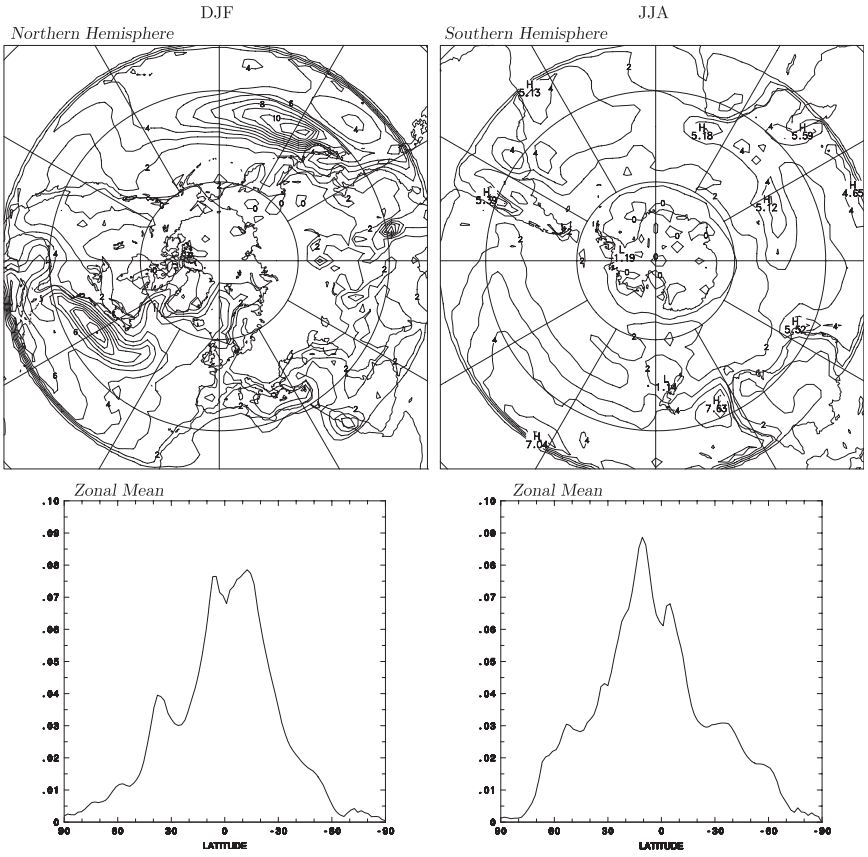

FIG. 9. (top) Distributions of the vertically integrated internal entropy production for (left) the DJF Northern Hemisphere and (right) the JJA Southern Hemisphere. Contour interval is 10^{-2} W m^{-2} K^{-1}. (bottom) Corresponding vertically integrated zonal mean results (W m^{-2} K^{-1}). Calculations are based on (8).

Fig. 10. It is found that the internal entropy production is primarily positive below the tropopause. Large positive values occur in the tropics and midlatitude regions (especially in the boundary layer) for both DJF and JJA. In such regions, the orderly temperature structures are undergoing strong dissipation by large-scale eddy flows and small-scale diabatic heat fluxes. In the stratosphere, though there are regions of negative internal entropy production similar to that of Fig. 7, the total result of the negative internal entropy production is negligible in comparison with that of the total positive result. The atmosphere as a whole does obey the second law of thermodynamics.

The internal entropy production due to large- and small-scale moisture diffusion and condensation/evaporation is given by

$$\sigma = -R_v \frac{J_{vi}}{\lambda} \frac{\partial \ln \overline{\mathcal{H}}}{\partial x_i} - R_v \frac{\overline{F}_l + \overline{F}_m}{\lambda} \frac{\partial \ln \overline{\mathcal{H}}}{\partial z} + R_v \rho (\overline{C - E}) \ln \overline{\mathcal{H}} \tag{16}$$

and is shown separately in the bottom panels of Fig. 10. The physical meaning for the second term is similar to the first term (as discussed above), except now it is for the unresolved small-scale moisture flux. The third term represents the irreversible processes of condensation and evaporation. It is shown that evaporation always corresponds to an increase of internal entropy under nonsaturated conditions ($\ln \overline{\mathcal{H}} < 0$) and to an unchanged internal entropy under saturated conditions ($\ln \overline{\mathcal{H}} = 0$), since the evaporation under the nonsaturated condition is irreversible. Condensation generally occurs when $\mathcal{H} > 1$; hence, it also corresponds to positive internal entropy production. Since condensation is an unresolved subgrid process, detailed correlations between condensation and relative humidity are not available for global climate reanalysis data. Because $\overline{\mathcal{H}}$ is a time-averaged grid mean result, it is generally less than 1. This leads to negative internal entropy production when condensation dominates over evaporation, that is, $\overline{C - E} > 0$. This contradicts the above statement that condensation corresponds to positive

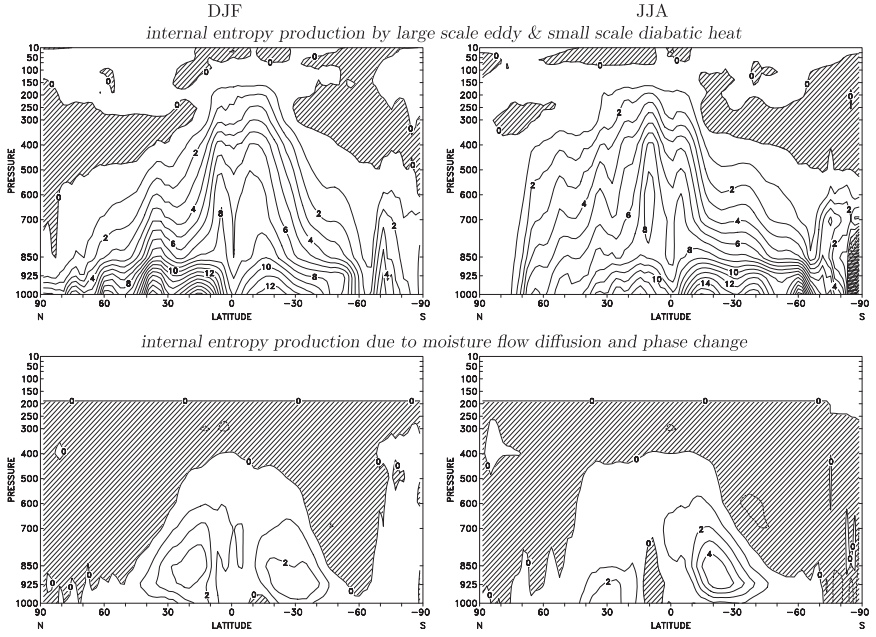

FIG. 10. (top) Zonal mean vertical distributions of total internal entropy production [by (8)] for (left) the DJF Northern Hemisphere and (right) the JJA Southern Hemisphere. (bottom) As in (top), but only for contributions from large-scale–small-scale moisture flow diffusions and phase change [from (16)]. Contour interval is 10^{-6} W m^{-3} K^{-1} with negative contours shaded.

internal entropy production. Generally, condensation occurs at $\mathcal{H}$ slightly over 1; thus, the value of ln $\mathcal{H}$ is positive but extremely small. Therefore, in regions dominated by condensation, the entropy production should be close to 0. Thus, the unresolved result of $\mathcal{H}$ has only a small influence on the distribution of internal entropy production.

In the bottom panels of Fig. 10, it is found that the internal entropy production due to moisture diffusion and phase change appears mostly in the tropics and subtropical high regions. The negative result appears in the tropical region due to the sink of convective moisture there. However, as shown in the bottom panels of Fig. 10, the total result of internal entropy production is positive in the tropical region.

The time evolution of the vertically integrated total internal entropy production by (8) is presented as dashed lines in Fig. 8. Compared to the large-scale eddy results (solid lines), the total internal entropy production is much larger, especially in the tropics. In the Northern Hemisphere, the dashed and solid lines are of opposite phases. The entropy production due to small-scale diabatic heating is larger in the summer season, while the entropy production due to large-scale eddies is larger in the winter season. In the Southern Hemisphere, the shift in phase becomes less. This is because the contribution due to large-scale eddies becomes smaller in the Southern Hemisphere, thus the diabatic heat contribution dominates in the total internal entropy production.

In Fig. 8, it is shown that the 10-yr averaged global mean vertically integrated value is 0.037 49 W m^{-2} K^{-1} for the total internal entropy production and 0.008 40 W m^{-2} K^{-1} for the large-scale eddy part. Pascale and Gregory (2009) obtained 0.0518 W m^{-2} K^{-1} for the total internal entropy production based on the calculation in the third climate configuration of the Met Office Unified Model (HadCM3). Also, Lucarini et al. (2011) obtained the results from 0.052 to 0.058 W m^{-2} K^{-1} for 13 climate models. The difference could be due to the different datasets from the NCEP reanalysis and from the climate model simulations. In addition, the approximate method of equivalent temperature was used in Pascale and Gregory (2009) and Lucarini et al. (2011). It is interesting to find that the internal entropy production due to a large-scale eddy is comparable to the horizontal part of the internal entropy production obtained in Lucarini et al. (2011), since the horizontal components dominate the large-scale eddy.

So far, we have not discussed the radiation contribution of $c_{pd}\rho\overline{Q}_r/\overline{T}$ in (6). The 10-yr-averaged global mean

$$\left\langle \int_0^{z_m} c_{\mathrm{pd}} \rho \frac{\overline{Q}_r}{\overline{T}} dz \right\rangle_g = -0.4241\ \mathrm{W\,m^{-2}\,K^{-1}},$$

where z_m is the height of 10 hPa. Using the correlated-k distribution radiation algorithm by Li and Barker (2005) with nonlocal thermodynamic equilibrium (non-LTE) correction in the mesosphere (Fomichev 2009), we obtained the global mean of

$$\left\langle \int_{z_m}^{z_t} c_{\mathrm{pd}} \rho \frac{\overline{Q}_r}{\overline{T}} dz \right\rangle_g = 0.025\,92\ \mathrm{W\,m^{-2}\,K^{-1}}.$$

This positive result is mostly from the ozone heating centered near the stratopause. Therefore, the global mean vertically integrated entropy production by radiation is -0.3982 W m^{-2} K^{-1}. In Table 1, it is shown that the total surface diabatic entropy flux is 0.3422 W m^{-2} K^{-1}. Figure 8 shows the vertically integrated internal entropy production is 0.037 49 W m^{-2} K^{-1}; also, the contribution above z_m is missing, but the value should be very small. The sum of the three values is very close to zero, which indicates the time-averaged global mean result of (6) holds in the atmosphere.

In this work, the entropy advection, $\rho\overline{u}_i\partial\overline{s}/\partial x_i$, has not been discussed. This term is close to zero for global mean. Locally, this term is not zero, but it plays an important role in the transport of entropy. This will be addressed in a subsequent paper.

5. Conclusions

The primary objective of this study was to investigate atmospheric entropy and its association with climate dissipation. The balance equation for entropy is derived using the mean and transient thermal and moisture equations. The external entropy production due to small-scale diabatic heat corresponds to the boundary entropy supply, which is determined by the unresolved small-scale diabatic heat fluxes. In the tropics, the net boundary supply of entropy is much larger than that in the extratropics. In the DJF Northern Hemisphere, there are two strong positive centers of boundary supply of entropy: one is in the northwestern Pacific and the other is in the northwestern Atlantic.

The external entropy production due to the large-scale eddy is the convergence of eddy entropy flow. Generally, the divergence of large-scale eddy entropy occurs in the lower latitudes and the convergence of large-scale eddy entropy occurs in the higher latitudes, which indicates the polarward transport of entropy flow.

The internal entropy production represents the physical process of dissipation. In the atmosphere, only in regions with strong thermal structure can strong dissipation occur. On the basis of this argument, we can determine the atmospheric temperature orderliness by the calculation of the distribution of internal entropy production. For the internal entropy production due to large-scale eddies only, there are informative patterns for the DJF Northern Hemisphere, with three contour centers in the western Pacific, the western Atlantic, and the north polar regions. This indicates that strong dissipation to the thermal and dynamic structures occurs in such regions. An interesting finding is that large-scale eddy internal entropy production is negative in the lower stratosphere, which corresponds to a process as the eddy flow moves counter to the gradient of temperature in this region. For the total internal entropy production due to the large-scale eddy flow and the small-scale diabatic heat flux, it is found that the internal entropy production is much larger in the tropical region than that in the extratropics, with a pattern similar to the surface entropy flux.

Acknowledgments. The authors thank Drs. C.-D. Johnson, S. Lambert, V. Lucarini, W. Merryfield, and anonymous reviewers for their constructive comments, and Dr. M. Shrinivas (at NCEP) for his help in interpreting NCEP data.

APPENDIX

Entropy Balance Equation

The continuity equation is

$$\frac{\partial \rho}{\partial t} + \frac{\partial(\rho u_i)}{\partial x_i} = 0,$$

where ρ is the air density. For flow in planetary atmospheres, the variation of density in the vertical direction is much larger than any horizontal fluctuations, and scale analysis shows that $\partial\rho/\partial t \ll \partial(\rho u_i)/\partial x_i$; thus, we have (James 1994) the following:

$$\frac{\partial(\rho u_i)}{\partial x_i} \approx 0. \tag{A1}$$

From (2), we have from (Emanuel 1994),

$$s \doteq c_{\mathrm{pd}} \ln\theta + \frac{\lambda q_v}{T} - R_v q_v \ln\mathcal{H} + s_0, \tag{A2}$$

where s_0 is a constant of integration. Given (A2) the mean entropy is

$$\begin{aligned}\bar{s} &= c_{\mathrm{pd}}\overline{\ln(\bar{\theta}+\theta')} + c_{\mathrm{pd}}\lambda\frac{\overline{q_v+q_v'}}{\overline{T}+T'} - R_v\overline{(\bar{q}_v+q_v')\ln(\overline{\mathcal{H}}+\mathcal{H}')} + \bar{s}_0\\ &= c_{\mathrm{pd}}\left(\overline{\ln\bar{\theta}+\frac{\theta'}{\bar{\theta}}}\right) + \lambda\overline{\frac{\bar{q}_v+q_v'}{\bar{T}}\left(1-\frac{T'}{\bar{T}}\right)} - R_v\overline{(\bar{q}_v+q_v')\left(\ln\overline{\mathcal{H}}+\frac{\mathcal{H}'}{\overline{\mathcal{H}}}\right)} + s_0\\ &= c_{\mathrm{pd}}\ln\bar{\theta} + \frac{\lambda\bar{q}_v}{\bar{T}} - R_v\bar{q}_v\ln\overline{\mathcal{H}} + \bar{s}_0. \end{aligned} \tag{A3}$$

In the derivation of (A3), terms proportional to $(\theta'/\bar{\theta})^n$, $(T'/\bar{T})^n$, and $(\mathcal{H}'/\overline{\mathcal{H}})^n$ for $(n \geq 2)$ are neglected, since they are at least one order smaller than that of terms $\sim 1/\bar{\theta}$ and $1/\bar{T}$. Also, the covariance term of $-R_v\overline{q_v'\mathcal{H}'}/\overline{\mathcal{H}}$ is neglected, since this term is found to be more than one order smaller than the mean relative humidity term. In (A3), the bar for a physical variable ψ is defined (James 1994) as

$$\overline{\psi} = \frac{1}{\tau}\int_0^\tau \psi\, dt,$$

where τ is the time length for the mean and the transient is $\psi' = \psi - \overline{\psi}$. We let $\rho = \bar{\rho}$. By Boussinesq approximation, ρ' becomes important only in a detailed process related to buoyancy. Given (A3)

$$\frac{\overline{d}\,\bar{s}}{dt} = \frac{c_{\mathrm{pd}}}{\bar{\theta}}\frac{\overline{d}\,\bar{\theta}}{dt} + \frac{\lambda}{\bar{T}}\frac{\overline{d}\,\bar{q}_v}{dt} - R_v\frac{\overline{d}\,\bar{q}_v}{dt}\ln\overline{\mathcal{H}} - R_v\bar{q}_v\frac{\overline{d}\ln\overline{\mathcal{H}}}{dt}, \tag{A4}$$

where $\overline{d}/dt = \partial/\partial t + \bar{u}_i\partial/\partial x_i$. In (A4), we neglect a term proportional to $1/\bar{T}^2$. Additionally, we neglect the last term on the right-hand side of (A4), since it is much smaller than the third term. The third term corresponds to a source of moisture flow and condensation–evaporation [see (A11)], whereas the last term does not. Applying (A1) to (A4) gives

$$\begin{aligned}\frac{\partial(\rho\bar{s})}{\partial t} + \frac{\partial(\rho\bar{u}_i\bar{s})}{\partial x_i} &= \frac{c_{\mathrm{pd}}}{\bar{\theta}}\left[\frac{\partial(\rho\bar{\theta})}{\partial t} + \frac{\partial(\rho\bar{u}_i\bar{\theta})}{\partial x_i}\right]\\ &\quad + \left(\frac{\lambda}{\bar{T}} - R_v\ln\overline{\mathcal{H}}\right)\left[\frac{\partial(\rho\bar{q}_v)}{\partial t} + \frac{\partial(\rho\bar{u}_i\bar{q}_v)}{\partial x_i}\right].\end{aligned} \tag{A5}$$

From Washington and Parkinson (2005),

$$\frac{T}{\theta}\frac{d\theta}{dt} = (Q_r + Q_h + Q_f + Q_1) + \frac{\lambda}{c_{\mathrm{pd}}}(C - E) \tag{A6}$$

where Q_r, Q_h, and Q_f are diabatic heating rates corresponding to radiation, sensible heating, and frictional heating, respectively; Q_1 is the heating rate for deep–shallow convection; and C and E are the condensation and evaporation rates, respectively. In NCEP data, the sensible heating rate corresponds to the turbulent vertical diffusion process. In (A6) Q_1 and $\lambda/c_{\mathrm{pd}}(C - E)$ are in the same category, but one is for convective scale and the other is for large scale, separately treated in NCEP data. Written in flux form, (A6) becomes

$$\begin{aligned}\frac{T}{\theta}\frac{d\theta}{dt} &= -\frac{1}{c_{\mathrm{pd}}\rho}\left(\frac{\partial F_h}{\partial z} - \rho\tau_{\alpha,3}\frac{\partial u_\alpha}{\partial z}\right) + Q_1\\ &\quad + \frac{\lambda}{c_{\mathrm{pd}}}(C - E) + Q_r\end{aligned} \tag{A7}$$

where F_h is the sensible heat flux and $\tau_{i,j}$ is the diffusion acceleration tensor (viscous stress). In (A7), we only keep the vertical components of the fluxes, since the vertical contribution dominates in diabatic heating. Similarly, the balance equation q_v from (Emanuel 1994)

$$\frac{dq_v}{dt} = -\frac{1}{\lambda\rho}\frac{\partial F_l}{\partial z} - \frac{c_{\mathrm{pd}}Q_2}{\lambda} + E - C, \tag{A8}$$

where F_l is the latent heat flux corresponding to the vertical turbulent moistening diffusion process, and Q_2/λ is the moistening rate for deep/shallow convection. Also $-c_{\mathrm{pd}}Q_2/\lambda$ and $E - C$ are in the same category but for different scales. The vertical diffusion moistening heating rate (latent heat) is $Q_l = -1/(c_{\mathrm{pd}}\rho)\partial F_l/\partial z$.

The terms Q_1 and Q_2 cannot be cancelled out because deep cumulus cloud can carry the released latent heat of condensation to the upper troposphere. Following Emanuel (1994),

$$Q_1 - Q_2 = -\frac{1}{\rho}\frac{\partial}{\partial z}(\rho[w^*h_v^*]),$$

where $[\cdot]$ and * represent the spatial mean and transient, respectively, and $[w^*h_v^*]$ is a turbulent flux. It is shown

$[w^*h_v^*] \approx 0$ at the surface for global mean due to the cancellation of updraft and downdraft flows. We denote $F_c = c_{pd}\rho[w^*h_v^*]$. Please note that in some treatments, other terms are lumped into Q_1 and Q_2. We restrict Q_1 and Q_2 to being only related to convection, the same as Emanuel (1994).

Decomposing to mean and transient and with the aid of (A1), (A7) and (A8) become

$$\frac{\partial(\rho\overline{\theta})}{\partial t} + \frac{\partial(\rho\overline{u}_i\overline{\theta})}{\partial x_i} = -\frac{\partial(\rho\overline{\theta' u_i'})}{\partial x_i} - \frac{1}{c_{pd}}\frac{\overline{\theta}}{\overline{T}}\left(\frac{\partial\overline{F}_h}{\partial z} - \rho\overline{\tau}_{3,\alpha}\frac{\partial\overline{u}_\alpha}{\partial z}\right) + \rho\frac{\overline{\theta}}{\overline{T}}(\overline{Q}_1 + \overline{Q}_r) + \frac{\overline{\theta}}{\overline{T}}\frac{\lambda\rho}{c_{pd}}\overline{(C-E)} \quad \text{and} \tag{A9}$$

$$\frac{\partial(\rho\overline{q}_v)}{\partial t} + \frac{\partial(\rho\overline{u}_i\overline{q}_v)}{\partial x_i} = -\frac{\partial(\overline{\rho q_v' u_v'})}{\partial x_i} - \frac{1}{\lambda}\frac{\partial\overline{F}_1}{\partial z} - \frac{c_{pd}\rho\overline{Q}_2}{\lambda} + \rho\overline{(E-C)}. \tag{A10}$$

Finally, we obtain the entropy balance equation for $\overline{s}$ by substituting (A9) and (A10) into (A5), giving

$$\frac{\partial(\rho\overline{s})}{\partial t} + \frac{\partial(\rho\overline{u}_i\overline{s})}{\partial x_i} = \frac{\overline{d}\rho\overline{s}}{dt} = -\frac{1}{\overline{\theta}}\frac{\partial J_{\theta i}}{\partial x_i} - \frac{1}{\overline{T}}\frac{\partial J_{vi}}{\partial x_i} + R_v\ln\overline{\mathcal{H}}\frac{\partial}{\partial x_i}\frac{J_{vi}}{\lambda} - \frac{1}{\overline{T}}\left(\frac{\partial\overline{F}_h}{\partial z} + \frac{\partial\overline{F}_l}{\partial z} + \frac{\partial\overline{F}_c}{\partial z} - \rho\overline{\tau}_{3,\alpha}\frac{\partial\overline{u}_\alpha}{\partial z}\right) + R_v\ln\overline{\mathcal{H}}\left[\frac{\partial}{\partial z}\frac{\overline{F}_l}{\lambda} + \rho\overline{(C-E)} + \frac{c_{pd}\rho\overline{Q}_2}{\lambda}\right] + c_{pd}\rho\frac{\overline{Q}_r}{\overline{T}}, \tag{A11}$$

where $J_{\theta i} = c_{pd}\rho\overline{\theta' u_i'}$ and $J_{vi} = \lambda\rho\overline{q_v' u_i'}$ are the large-scale eddy thermal flow and the moistening heat flow, respectively. We call J_{vi}/λ the large-scale eddy moisture flow and F_i/λ the small-scale moisture flux.

If we neglect the terms related to large-scale eddy and $\ln\overline{\mathcal{H}}$, we have

$$\frac{\overline{d}\rho\overline{s}}{dt} = c_{pd}\rho\frac{\overline{Q}_{diab}}{\overline{T}} + c_{pd}\rho\frac{\overline{Q}_r}{\overline{T}}, \tag{A12}$$

where $\overline{Q}_{diab} = (-1/c_{pd}\rho)[(\partial\overline{F}_h/\partial z) + (\partial\overline{F}_l/\partial z) + (\partial\overline{F}_c/\partial z) - \rho\overline{\tau}_{3,\alpha}(\partial\overline{u}_\alpha/\partial z)]$ is the total diabatic heating rate. Equation (12) is equivalent to the balance equation (10) in Goody (2000).

By separating the entropy production into the external and internal part, we have

$$\frac{\overline{d}\rho\overline{s}}{dt} = -\frac{\partial}{\partial x_i}\left(\frac{J_{\theta i}}{\overline{\theta}} + \frac{J_{vi}}{\overline{T}} - R_v\frac{J_{vi}}{\lambda}\ln\overline{\mathcal{H}}\right) - \frac{\partial}{\partial z}\left(\frac{\overline{F}_h}{\overline{T}} + \frac{\overline{F}_l}{\overline{T}} + \frac{\overline{F}_c}{\overline{T}} - \frac{\rho\overline{u}_\alpha\overline{\tau}_{3,\alpha}}{\overline{T}} - R_v\frac{\overline{F}_l + \overline{F}_m}{\lambda}\ln\overline{\mathcal{H}}\right) + \sigma + c_{pd}\rho\frac{\overline{Q}_r}{\overline{T}}. \tag{A13}$$

In the right-hand side of (A13), the first two terms are the external entropy production and

$$\sigma = J_{\theta i}\frac{\partial}{\partial x_i}\frac{1}{\overline{\theta}} + J_{vi}\frac{\partial}{\partial x_i}\frac{1}{\overline{T}} - R_v\frac{J_{vi}}{\lambda}\frac{\partial\ln\overline{\mathcal{H}}}{\partial x_i} + (\overline{F}_h + \overline{F}_l + \overline{F}_c)\frac{\partial}{\partial z}\frac{1}{\overline{T}} - \overline{u}_\alpha\frac{\partial}{\partial z}\left(\frac{\rho\overline{\tau}_{3,\alpha}}{\overline{T}}\right) - R_v\frac{\overline{F}_l + \overline{F}_m}{\lambda}\frac{\partial\ln\overline{\mathcal{H}}}{\partial z} + R_v\rho\overline{(C-E)}\ln\overline{\mathcal{H}} \tag{A14}$$

is the internal entropy production, where $\overline{F}_m$ is the moistening heat flux corresponding to Q_2, with $\overline{Q}_2 = 1/(c_{pd}\rho)(\partial F_m/\partial z)$].

REFERENCES

de Groot, S. R., and P. Mazur, 1984: *Non-Equilibrium Thermodynamics*. Dover, 510 pp.

Emanuel, K. A., 1994: *Atmospheric Convection*. Oxford University Press, 580 pp.

Fomichev, V., 2009: The radiative energy budget of the middle atmosphere and its parameterization in general circulation models. *J. Atmos. Terr. Phys.,* **71,** 1577–1585.

Fraedrich, K., and F. Lunkeit, 2008: Diagnosing the entropy budget of a climate model. *Tellus,* **60A,** 921–931, doi:10.1111/j.1600-0870.2008.00338.x.

Goody, R., 2000: Sources and sinks of climate entropy. *Quart. J. Roy. Meteor. Soc.,* **126,** 1953–1970.

——, 2007: Maximum entropy production in climate theory. *J. Atmos. Sci.,* **64,** 2735–2739.

Held, I., 1999: The macroturbulence of the troposphere. *Tellus,* **51B,** 59–70.

Iribarne, J. V., and W. L. Godson, 1981: *Atmospheric Thermodynamics*. 2nd ed. Kluwer, 259 pp.

James, I. N., 1994: *Introduction to Circulating Atmospheres*. Cambridge Atmospheric and Space Science Series, Cambridge University Press, 422 pp.

Johnson, D. R., 1997: General coldness of climate models and the second law: Implications for modeling the earth system. *J. Climate,* **10,** 2826–2846.

Kistler, R., and Coauthors, 2001: The NCEP–NCAR 50-Year Reanalysis: Monthly means CD-ROM and documentation. *Bull. Amer. Meteor. Soc.,* **82,** 247–267.

Li, J., 2009: On the extreme of internal entropy production. *J. Phys.,* **42A,** 035002, doi:10.1088/1751-8113/42/3/035002.

——, and H. W. Barker, 2005: A radiation algorithm with correlated-*k* distribution. Part I: Local thermal equilibrium. *J. Atmos. Sci.,* **62,** 286–309.

Liu, C., and Y. Liu, 2004: Negative entropy flow and its effect on the organization of synoptic-scale severe atmospheric systems. *Geophys. Res. Lett.,* **31,** L01108, doi:10.1029/2003GL018071.

Lorenz, R. D., J. I. Lunine, P. G. Withers, and C. P. McKay, 2001: Mars and earth: Entropy production by latitudinal heat transport. *Geophys. Res. Lett.,* **28,** 415–418.

Lucarini, V., 2009: Thermodynamic efficiency and entropy production in the climate system. *Phys. Rev.,* **80,** 021118, doi:10.1103/PhysRevE.80.021118.

——, K. Fraedrich, and F. Lunkeit, 2010: Thermodynamic analysis of snowball earth hysteresis experiment: Efficiency, entropy production, and irreversibility. *Quart. J. Roy. Meteor. Soc.,* **136,** 2–11.

——, ——, and F. Ragone, 2011: New results on the thermodynamical properties of the climate system. *J. Atmos. Sci.,* **68,** 2438–2458.

Nicolis, G., and C. Nicolis, 1980: On the entropy balance of the earth-atmosphere system. *Quart. J. Roy. Meteor. Soc.,* **106,** 691–706.

O'Brien, D. M., and G. L. Stephens, 1995: Entropy and climate. II: Simple models. *Quart. J. Roy. Meteor. Soc.,* **121,** 1773–1796.

Ou, H.-W., 2001: Possible bounds on the earth's surface temperature: From the perspective of a conceptual global-mean model. *J. Climate,* **14,** 2976–2988.

Ozawa, H., A. Ohmura, R. D. Lorenz, and T. Pujol, 2003: The second law of thermodynamics and the global climate system: A review of the maximum entropy production principle. *Rev. Geophys.,* **41,** 1–24.

Paltridge, G. W., 1975: Global dynamics and climate - A system of minimum entropy exchange. *Quart. J. Roy. Meteor. Soc.,* **101,** 475–484.

Pascale, S., J. M. Gregory, M. Ambaum, and R. Tailleux, 2009: Climate entropy budget of the HadCM3 atmosphere–ocean general circulation model and of FAMOUS, its low-resolution version. *Climate Dyn.,* **36,** 1189–1206, doi:10.1007/s00382-009-0718-1.

Pauluis, O., and I. M. Held, 2002a: Entropy budget of an atmosphere in radiative convective equilibrium. Part I: Maximum work and frictional dissipation. *J. Atmos. Sci.,* **59,** 125–139.

——, and ——, 2002b: Entropy budget of an atmosphere in radiative convective equilibrium. Part II: Latent heat transport and moist processes. *J. Atmos. Sci.,* **59,** 140–149.

Peixoto, J. P., and A. H. Oort, 1992: *Physics of Climate*. American Institute of Physics, 520 pp.

Prigogine, I., 1980: *From Being to Becoming: Time and Complexity in the Physical Sciences*. W. H. Freeman, 272 pp.

Pujol, T., and J. E. Llebot, 1999a: Extremal principle of entropy production in the climate system. *Quart. J. Roy. Meteor. Soc.,* **125,** 79–90.

——, and ——, 1999b: Second differential of the entropy as a criterion for the stability in low-dimensional climate models. *Quart. J. Roy. Meteor. Soc.,* **125,** 91–106.

Shimokawa, S., and H. Ozawa, 2007: Thermodynamics of irreversible transitions in the oceanic general circulation. *Geophys. Res. Lett.,* **34,** L12606, doi:10.1029/2007GL030208.

Takamitsu, I., and A. Kleidon, 2005: Entropy production of atmospheric heat transport. *Non-Equilibrium Thermodynamics and the Production of Entropy: Life, Earth, and Beyond,* A. Kleidon and R. D. Lorenz, Eds., Understanding Complex Systems, Springer, 93–106.

Wallace, J. M., 1978: Trajectory slopes, countergradient heat fluxes and mixing by lower stratospheric waves. *J. Atmos. Sci.,* **35,** 554–558.

Washington, W. M., and C. L. Parkinson, 2005: *An Introduction to Three-Dimensional Climate Modeling*. 2nd ed. University Science Books, 353 pp.